



This is a repository copy of *Smart soils track the formation of pH gradients across the rhizosphere.*

White Rose Research Online URL for this paper:

<https://eprints.whiterose.ac.uk/205635/>

Version: Published Version

Article:

Patko, D., Yang, Q., Liu, Y. et al. (9 more authors) (2023) Smart soils track the formation of pH gradients across the rhizosphere. *Plant and Soil*. pp. 1-14. ISSN 0032-079X

<https://doi.org/10.1007/s11104-023-06151-y>

Reuse

This article is distributed under the terms of the Creative Commons Attribution (CC BY) licence. This licence allows you to distribute, remix, tweak, and build upon the work, even commercially, as long as you credit the authors for the original work. More information and the full terms of the licence here:

<https://creativecommons.org/licenses/>

Takedown

If you consider content in White Rose Research Online to be in breach of UK law, please notify us by emailing eprints@whiterose.ac.uk including the URL of the record and the reason for the withdrawal request.



eprints@whiterose.ac.uk
<https://eprints.whiterose.ac.uk/>



Smart soils track the formation of pH gradients across the rhizosphere

Daniel Patko · Qizhi Yang · Yangminghao Liu · Panagiotis Falireas · Benoit Briou · Bhusaheb V. Tawade · Timothy S. George · Tim J. Daniell · Michael P. MacDonald · Vincent Ladmiral · Bruno Ameduri · Lionel X. Dupuy 

Received: 4 January 2023 / Accepted: 29 June 2023
© The Author(s) 2023

Abstract

Aims Our understanding of the rhizosphere is limited by the lack of techniques for in situ live microscopy. Current techniques are either destructive or unsuitable for observing chemical changes within the pore space. To address this limitation, we have developed artificial substrates, termed smart soils, that enable the acquisition and 3D reconstruction of chemical sensors attached to soil particles.

Methods The transparency of smart soils was achieved using polymer particles with refractive index matching that of water. The surface of the particles was modified both to retain water and act as a local sensor to report on pore space pH via fluorescence emissions. Multispectral signals were acquired from the particles using a light sheet microscope, and machine learning algorithms predicted the changes and spatial distribution in pH at the surface of the smart soil particles.

Results The technique was able to predict pH live and in situ within ± 0.5 units of the true pH value. pH distribution could be reconstructed across a volume of several cubic centimetres around plant roots at 10 μm resolution. Using smart soils of different composition, we revealed how root exudation and pore structure create variability in chemical properties.

Responsible Editor: Yinglong Chen.

Daniel Patko, Qizhi Yang, Yangminghao Liu and Panagiotis Falireas contributed equally to this work.

Supplementary information The online version contains supplementary material available at <https://doi.org/10.1007/s11104-023-06151-y>.

D. Patko · Y. Liu · T. S. George · L. X. Dupuy (✉)
Ecological Sciences, The James Hutton Institute,
Dundee DD2 5DA, UK
e-mail: ldupuy@neiker.eus

D. Patko · L. X. Dupuy
Department of Conservation of Natural Resources, Neiker,
Derio 48160, Spain

Q. Yang · P. Falireas · B. Briou · B. V. Tawade ·
V. Ladmiral · B. Ameduri (✉)
Ingénierie et Architectures Macromoléculaires, Institut
Charles Gerhardt, CNRS, University of Montpellier,
ENSCM, Montpellier 34000, France
e-mail: bruno.ameduri@enscm.fr

Y. Liu · M. P. MacDonald
School of Science and Engineering, University of Dundee,
Dundee DD1 4HN, UK

T. J. Daniell
Plants, Photosynthesis and Soil, School of Life Sciences,
The University of Sheffield, Sheffield S10 2TN, UK

L. X. Dupuy
Ikerbasque, Basque Foundation for Science, Bilbao 48009,
Spain

Conclusion Smart soils captured the pH gradients forming around a growing plant root. Future developments of the technology could include the fine tuning of soil physicochemical properties, the addition of chemical sensors and improved data processing. Hence, this technology could play a critical role in advancing our understanding of complex rhizosphere processes.

Keywords Sensing soil · Root · Rhizosphere · Light sheet microscopy · Live imaging

Introduction

Studies of dynamic rhizosphere processes in soil are challenging. Direct observations and the use of optical microscopes are limited because soils block electromagnetic signals in the visible domain and invasive approaches permanently disrupt the functioning of communities of biological organisms. The radio waves used in ground penetrating radars can penetrate soils, but cannot resolve micrometric variation (Jol 2008). The application of penetrating radiation such as X-ray or neutron tomography successfully depict the physical structure of soils non-destructively (Moradi et al. 2011; Koebernick et al. 2019; Burr-Hersey et al. 2020), but biological or geochemical processes are more difficult to detect. Techniques such as X-Ray fluorescence provide insights into the chemical structures of soil (Van Veelen et al. 2020) and recent advances in X-Ray microscopy now enable the resolution of small biological structures such as plant anatomical features (Duncan et al. 2022). However, there are limitations on the use of such techniques in real-time experiments due to both the radiation doses required and the time needed to acquire each time point (Zappala et al. 2013).

Since *in vivo* observations are rendered impractical in natural soils, the use of artificial media as model systems have become central to rhizosphere studies. Liquid cultures offer simple ways to monitor root growth while sampling for compounds released by roots and microbes (Oburger and Jones 2018). However, these systems lack the physical support and physical/chemical heterogeneity of a matrix to allow microbes to establish in the root surroundings. Experiments in hydroponic systems create homogeneous conditions that significantly decrease the richness and

diversity of microbial communities (Korenblum et al. 2020). Growth substrates, such as hydrogels, can mimic the mechanical resistance of soils (Clark et al. 1999) and facilitate biochemical studies of the rhizosphere through inclusion of indicator dyes (Kopittke and Menzies 2004) or the use of techniques such as microdialysis extraction (Plett et al. 2021). But hydrogels also lack physical heterogeneity and cannot be aerated with hypoxic conditions developing with depth due to the slow diffusion of oxygen (Van der Meeren et al. 2001).

Recent studies have demonstrated the possibility of culturing and observing soil organisms in transparent soils (Downie et al. 2012; O’Callaghan et al. 2018; Ma et al. 2019; Sharma et al. 2020). Transparent soils are artificial substrates composed of solid particles whose refractive index matches that of water such that light can penetrate the substrate without significant scattering, reflection and refraction by the soil particles. Live observations of biological activity can then be made in the pore space between soil particles (Liu et al. 2021; Engelhardt et al. 2022), and physical manipulations such as ablation or cell guiding can be achieved using lasers (Ge et al. 2021), for example to control the number of bacterial cells attached to a specific plant tissue (Ge et al. 2023).

Rhizosphere research has also greatly benefitted from the recent development of optochemical sensors, notably planar optodes and zymography. A layer of analyte sensitive material is applied at the surface of the soil, and changes in fluorescence intensity, fluorescence lifetime, transmittance, or colour can be captured by a camera and correlated to soil chemical composition (Baldini et al. 2006; Blossfeld and Gansert 2007). The technique is now widely used to study changes in chemical activity along plant roots, including pH (Koop-Jakobsen et al. 2018; Sun et al. 2019), oxygen (Han et al. 2016; Rudolph-Mohr et al. 2021) or ammonium (Strömberg 2008), and to report on the activity of various types of enzymes (Giles et al. 2018). Optodes also exist for the detection of nitrate (Huber et al. 2001) and potassium (Lookadoo et al. 2021) but these have not yet been applied to the soil environment. As a result of these optochemical sensors being applied at the surface of the soil, measurements may not correlate well with actual soil properties *in situ*. Therefore, a possible next step is to engineer the transparent soil particles themselves to enable the acquisition of optical signals reporting on

soil conditions locally and at the microscopic scale (Fig. 1). We termed these substrates smart soils.

Here we present the development of the first generation of such smart soils. The approach proposed is to use FEP (Fluorinated Ethylene Propylene), a low cost and low refractive index fluoropolymer and combines it with optochemical sensors that measure chemical properties at the surface of smart soil particles. We have optimised the smart soils for root growth and measurement of rhizosphere pH, an important indicator of nutrient availability, plant stress and soil function. We demonstrate acquisition of multispectral signals in situ from the smart soil particles using light sheet microscopy and assess how the pore structure and root exudation contribute to the formation of pH heterogeneity in soil.

Materials and methods

FEP core particles

FEP (Fluorinated Ethylene Propylene or *poly(tetrafluoroethylene-co-hexafluoropropylene)*) copolymer is a plastic commonly produced by industries for tubing, coatings, and cable manufacturing (Ebnesajjad 2015). Particles were obtained from the factory (Holscott, UK) in the form of pellets (virgin material used for extrusion) and chunks (factory waste). Chunk FEP particles were sieved to remove particles above 1.25 mm. Both types of particles were treated in oxygen plasma at 100 W for 1 min

(HPT-100, Henniker, UK) to remove dust and other surface residues before further chemical processing.

Synthesis and characterisation

FEP and fluoropolymers in general have characteristics critical for application to optochemical sensing, e.g. they have both a low refractive index and high transparency (Hougham et al. 1999; Okamoto et al. 2014; Ameduri and Fomin 2020). They are also chemically inert and have properties such as photostability along with great chemical, thermal and oxidation resistance (Dams and Hintzer 2016; Henry et al. 2018). Because FEP is transparent and has a refractive index of 1.341–1.347 (DuPont 2013), the particle allows index matching in the smart soil interstices with water and subsequent acquisition of fluorescent signal from the inner pore structure. However, some properties, such as hydrophobicity and chemical stability make them challenging for use as a soil substitute. Here, we synthesize polymers that can transform the properties of FEP to increase the hydrophilicity of the surface for improved retention of water, and to include an optochemical sensor for the detection of pH gradients.

Reagents consisted of 2,2,2-trifluoroethyl α -fluoroacrylate (FATRIFE) and hexafluoroisopropyl α -fluoroacrylate (FAHFIP) purchased from Scientific Industrial Application P and M (Russia). These fluorinated monomers were used to increase the fluorine content of the terpolymer and increase the likelihood of fluorine-fluorine interaction with

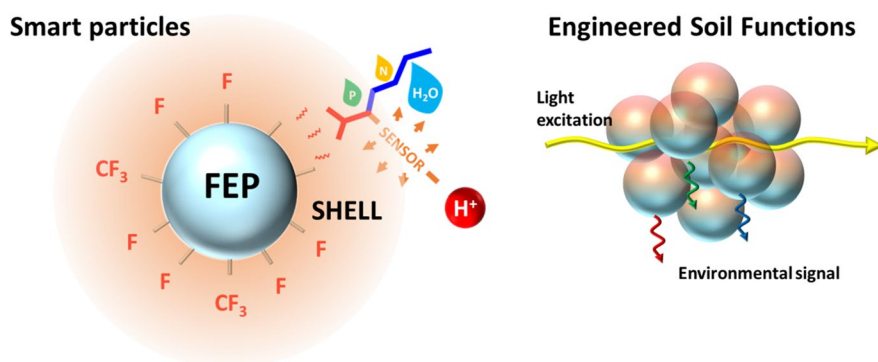


Fig. 1 Smart soil particles are made of a core made of waste Fluorinated Ethylene Propylene (FEP), which is embedded into a functional terpolymer, the shell (left). The shell holds water and nutrients and includes a sensor (here a pH sensor). The soil

is subsequently able to respond to external stimuli such as light of various wavelength to report on processes affecting the shell (right)

FEP (Baker et al. 2012; Panini and Chopra 2015; Pigliacelli et al. 2022). Oligo(ethylene glycol) methyl ether methacrylate ($M_n = 300$ g/mol), Nile Blue A (> 75%), acryloyl chloride (97%), methyl ethyl ketone (MEK) and acetonitrile were purchased from (Sigma Aldrich, France) while *tert*-butyl peroxyvalate (TBPPi, 75%) was gifted by Akzo Nobel (France). Nile Blue methacrylate (NBMA) was synthesized according to a previous report (Alcantar et al. 2000). Poly(FATRIFE-*ter*-PEGMA-*ter*-NBMA) terpolymers were characterized by ^1H and ^{19}F NMR spectroscopies (AC 400 spectrometer, Bruker, France) and size exclusion chromatography (model 210, Varian Prostar, France) using 0.1 M LiBr/DMF as the eluent, calibrated with PMMA narrow standards. Fourier transform infrared spectroscopy (FTIR) analyses were performed in the Attenuated Total Reflectance (ATR) mode (Spectrum 1000, Perkin-Elmer, France). Thirty two scans were carried out on a selection of particles, at wavelengths between 400 and 4000 cm^{-1} with a resolution of ± 2 cm^{-1} . “The synthesis of poly(FATRIFE-*ter*-PEGMA-*ter*-NBMA) terpolymers was achieved by conventional radical polymerization. A 50 ml round bottom flask equipped with a condenser and a magnetic stirring bar was filled with TBPPi (0.101 g, 0.57 mmol), FATRIFE (4.94 g, 28.70 mmol), PEGMA (8.60 g, 28.70 mmol), NBMA (29 mg, 0.057 mmol), TBPPi (0.101 g, 0.57 mmol) and 32 ml DMF. The reaction medium was deoxygenated by bubbling with nitrogen for 15 mins and then placed into an oil bath at 56°C. Terpolymerization was stopped after 4 hours by immersing the flask in liquid nitrogen and exposing its content to air. The crude product was purified by precipitation from water, filtering and lyophilisation (81% yield) prior to characterisation by ^1H , ^{19}F and IR spectroscopies.

Preparation of fluorinated ethylene-propylene [poly(tetrafluoroethylene-co-hexafluoropropylene FEP) particles

In the next step, FEP particles were coated with the functional polymer to modify the surface properties of the particles. 0.40 g of poly(FATRIFE-*ter*-PEGMA-*ter*-NBMA) terpolymer was dissolved in 25 ml methyl-ethyl ketone (25642.325, VWR, UK) in a 500 ml rotary evaporator flask containing 20 g of FEP at 40 °C. The rotation speed was increased progressively during the evaporation of the solvent to reach a

speed of 240 rpm. Particles were then dried overnight at 40 °C. The use of solvent during the coating maintained sterility (Hoell et al. 2012). To test for coating stability, particles were placed in a test tube immersed in water and spun horizontally at room temperature for several weeks. Then, the particles were filtered and dried in an oven for 12 h at 40 °C and analysed by FTIR spectroscopy as described above. Water contact angle measurements were performed with a contact angle goniometer (OCA contact angle system, Neutrek Instruments, Spain). Water retention curves for the chunk and pellet FEP particles (packed loosely at a density of approximately 0.5 g cm^{-3}), as well as for the functional terpolymer were obtained using a sandbox system (Sandbox 08.01, Eijkelkamp, Netherlands). Samples were weighed daily, and water tension was adjusted when no loss was recorded between two measurements. The water tension applied varied from 0 kPa to 8 kPa in intervals of 0.25 kPa initially and increasing progressively to 0.85 kPa. Spectral properties of the polymers were characterised using a standard multiplate reader (Variokan™ LUX Multimode, Thermo Scientific, UK).

Plant material and growth conditions

Lettuce (*Lactuca sativa*) cv. all year round (Sutton Seeds, UK) seedlings were sterilised in 10% bleach for 20 min and then washed 6 times in sterile dH_2O (O’Callaghan et al. 2018). Then the seeds were placed on the surface of 1% water agar gel in a Petri dish under a laminar air flow cabinet to maintain axenic conditions, and were then kept at 20 °C for 24 h wrapped in aluminium in an incubator. After germination, the seedlings were planted into mesocosm chambers on the surface of the substrate under sterile conditions.

Biocompatibility assays were performed with chunk FEP particles, fine sand (Pennine Aggregates, MS01 0001), agricultural soil (Cambisol, Sandy loam, 71% sand, 19% silt and 10% clay, Dundee, 56°27’34.8” N 3°4’21.01”W) and water agar (1%, Sigma A1296-100G). For smart soil, 1.4 cm^3 of substrate were introduced in glass vials (75 mm x 9 mm) and 0.8 ml of half MS liquid solution (pH 7, Sigma-Aldrich M5519) was added. For the other soils, 1.4 cm^3 of substrate were introduced in glass vials and 0.3 ml of distilled water was added. Sterilised lettuce seeds were grown at 21 °C for 12 days with 16 h light and 8 h dark period. Plants were harvested for

measurement of shoot dry weight and root length at the end of the experiment.

For imaging, mesocosm chambers consisted of two glass slides ($76 \times 26 \times 1$ mm, VWR) separated by a 3 mm thick-spacer made of Polydimethylsiloxane (PDMS) were constructed as described by Liu et al. (2021). Smart soil was added to the microcosms and compacted by gentle tamping. Two thirds of the mesocosm chambers were filled with smart soil. 1.5 ml of half MS liquid solution was added. The smart soils were therefore imaged unsaturated. Following planting the mesocosms were sealed with parafilm tape. The mesocosms were kept in an incubator at 20 °C with 16 h light period ($60 \mu\text{mol}/\text{mm}^2\text{s}$) and 8 h dark period. Plants were grown for one week (ensuring that the roots did not reach the bottom of the mesocosm chamber) after which the analysis of the spatial distribution of pH was performed. For live imaging 10 samples were sown in total. 5 lettuce plants grew in chunk FEP particles and 5 lettuce plants grew in pellet FEP particles. Additional time lapse imaging was carried out on one sample for illustration purposes.

Quantitative imaging

The mesocosms contained a mixture of nutrient solution, air and smart soil particles. Although the water added increased the transparency, air remaining within the pores of smart soils caused significant challenges for imaging due to the reflection and scattering of light. To address this challenge, we develop a live imaging method based on the Light Sheet Fluorescence Microscope (LSFM) developed by Liu et al. (2021). In short, a thin sheet of light was created using a laser source. The light sheet passed through the sample with the microscope objective and digital camera placed perpendicular to the light sheet to capture light emitted from the sample either through scattering or fluorescence at maximum dynamic range (16 bits). Long pass filters were used so that only fluorescence signals were collected. The camera collected a 2D cross section of the fluorescence signal emitted by the sample. A motorised stage was then used to acquire 2D cross sections across the whole sample so that a complete 3D reconstruction of the pore structure could be achieved. The system was equipped with a four wavelength-laser source (Vortran Versalase, Laser 2000 Ltd, UK) with wavelengths of 488 nm, 514 nm,

561 and 633 nm with the imaging arm fitted with long pass filters of 530 nm, 570 nm, 645 and 665 nm, respectively (Thorlabs FGL530, FGL570, FGL645, FGL665). The signal corresponding to each fluorescence signal was recorded in separate images noted $I_i \in \{488 \text{ nm}, 514 \text{ nm}, 561 \text{ nm and } 633 \text{ nm}\}$. For example, I_{488} represents the fluorescent signal collected when 488nm wavelength laser was used in combination with a long pass filter of 530 nm. I_i is not a scalar quantity but a function of the position in the x-y plane of the image so that $I_i(x, y)$ is the pixel intensity collected at positions x and y from laser excitation at wavelength i .

A dataset was assembled to calibrate pH predictions. Samples contained only smart soils kept at 11 different pH levels achieved using MES acid monohydrate and Na buffers (1.06126 and 1.06197, Merck, UK) at respective pH of 4.97, 5.20, 5.37, 5.58, 5.78, 6.03, 6.18, 6.38, 6.63, 6.80 and 6.97. Image data were collected from 3 experimental runs. Four Images were collected for each pH and for each of the four wavelengths (i.e. 44 images for each location measured). Points of interests were automatically extracted from images obtained at 488 nm excitation and 530 nm emission (Fig. S1). These points were then used to collect a dataset describing the relation between pixel intensities at all wavelengths and pH values. Regressions were established between pH and image intensity ratios $\text{pH} = f\left(\frac{I_i}{I_j}\right), i \neq j$ (Fig. S2). To further improve predictions, neural network models of the type $\text{pH} = f(I_i, x, y)$, were developed using a Multi-layer Perceptron regressor with rectified linear unit function and trained using a Limited-memory BFGS optimiser. The final neural network model contained 3 layers of 12 neurons each (Fig. S3 and S4).

Computation and statistical analysis

Computations were performed using the Scikit-learn library (Pedregosa et al. 2011). Datasets of pixel intensity at known pH was compiled with macros and scripts developed in ImageJ. Analysis of Variance and Tuckey's Post Hoc tests were performed in the R software package with a statistical significance level 0.05. Analysis of pH variations surrounding plant roots was done using the nlme library (Pinheiro et al. 2013).

Results

Functionalisation of Fluoropolymers allows fabrication of smart soil particles

This study has successfully used waste FEP (Fluorinated Ethylene Propylene or *poly(tetrafluoroethylene-co-hexafluoropropylene)* copolymer for the design of smart soil particles. Waste FEP particles were coated with a thin polymer shell augmenting them with a range of custom properties (Fig. 1). The design of the shell was achieved by conventional radical terpolymerisation of three comonomers, each of them bringing specific and complementary properties. We synthesised and trialled numerous materials (Supplementary Information 1) and can conclude that key elements are needed for successful use of smart soils as a plant growth medium. First, a fluoropolymer matrix was required for bonding, since it is known that Fluorine-Fluorine specific interactions are possible. 2,2,2-trifluoroethyl α -fluoroacrylate (FATRIFE) monomer were used, but similar attachment could be obtained with hexafluoroisopropyl α -fluoroacrylate (FAHFIP). Plant growth also requires the particle to retain water and nutrients at the surface of the particle. Because of the hydrophobic behaviour of FEP and fluoroalkyl α -fluoroacrylates, hydrophilicity was achieved by addition of either carboxylic acids (brought by 2-trifluoromethyl acrylic acid (MAF) or methacrylic acid) or oligo(ethylene oxide) groups. Finally, the use of sensors for acquisition of biological or environmental signals, was demonstrated with the addition of dyes based on fluorescein and Nile Blue. The terpolymerisation of FATRIFE with polyethylene glycol methacrylate (PEGMA) and Nile blue methacrylate (NBMA), initiated by *tert*-butyl peroxyvalate (TBPPi), resulted in a wide range of terpolymers the compositions of which were determined by ^1H and ^{19}F NMR spectroscopy.

Functional materials improve growth conditions and allow attachment of pH sensor

The main polymer tested in this study was poly(FATRIFE-*ter*-PEGMA-*ter*-NBMA) terpolymer with 75/25/0.1 molar ratio (Fig. 2A). Fourier-transform infrared spectroscopy (FTIR) of the coating demonstrated the successful deposition of the material on the surface of the particles (Fig. 2B).

The coating produced strong adhesion on the FEP which resisted two months of spinning in water. The particles were subsequently tested for their ability to deliver optical signals using a light sheet microscope (Fig. 2C). The coating drastically reduced the water contact angle of FEP particles and therefore increased the ability of the substrate to hold water. The water contact angle measured for uncoated particles was $108.8 \pm 0.5^\circ$ ($n=6$). By comparison, the water contact angle measured on particles coated with the functional polymer was $46.3 \pm 2.1^\circ$ ($n=6$) (Fig. 2D). Once assembled into its granular form loose and unpacked, the smart soil had a density of $0.537 \pm 0.08 \text{ g/cm}^3$ ($n=6$). Since solid FEP has a density of 2.150 g/cm^3 , the estimated porosity of the smart soil was 75%. The increased wettability of the particle surfaces following coating led to much improved water retention (Fig. 2E). The smart soils were trialled for biocompatibility. An Analysis of Variance showed the type of substrate did not have a significant effect on the shoot biomass ($p=0.25$). However, the type of substrate had an effect on the morphology of the root system ($p<0.05$). Plants grown in soil produced larger root systems while plants grown in sand produced the smallest root systems. The root systems of plants grown in smart soil were shorter than those of plants grown in soil, and not statistically different from those of plants grown in gel (Fig. 3). Further characterisation of polymer is presented in the [Supplementary Information](#).

Multispectral light sheet imaging resolves pH changes at the micro-scale, live and *in situ*

Although particles showed consistent changes in fluorescent intensity, the response varied significantly between individual particles (Fig. 4A). To overcome this feature, a ratiometric fluorescence approach was first attempted, but this yielded pH predictions with limited accuracy (Figure S2). The best results with ratiometric fluorescence were obtained with light excitation at 488 nm and 633 nm and calculation of prediction intervals showed 95% predictions of pH values were within ± 0.5 units of the true pH value. Machine learning proved more successful. Here we used four illumination wavelengths (488 nm, 514 nm, 561 and 633 nm). For each wavelength a fluorescent signal was recorded and a neural network model used to

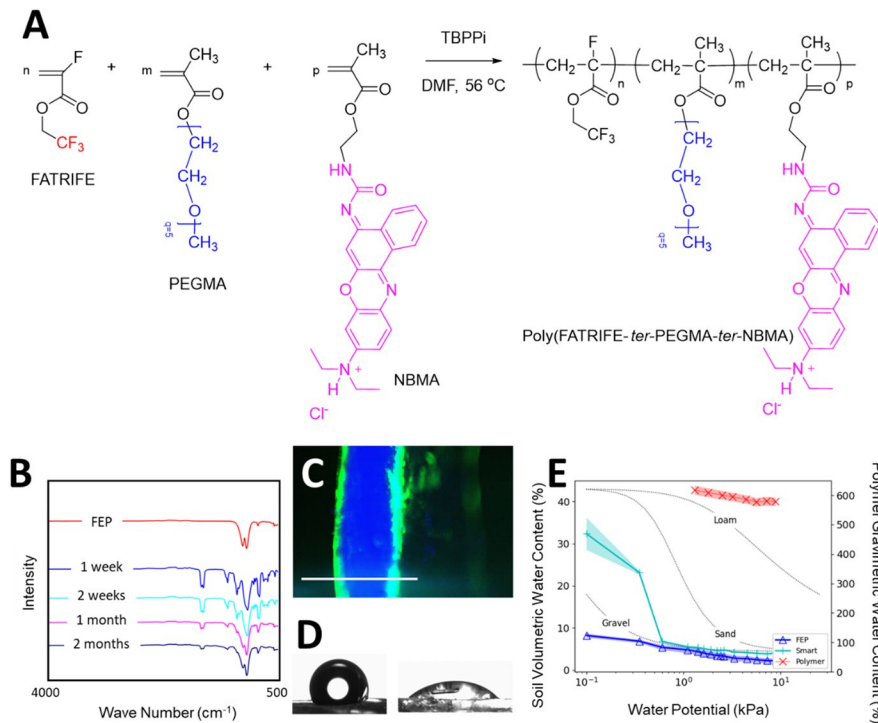


Fig. 2 Using FEP particles for the fabrication of smart soil particles. **A** Chemical structure of the polymeric shell material encoding three different functions. The polymer consisted of α -fluoro-2,2,2-trifluoroacrylate (FATRIFE) for the attachment onto the FEP core, PEGMA (Polyethyleneglycol methacrylate) enhanced water retention and Nile Blue methacrylate (NBMA) brought the pH sensor. Materials were tested for various properties during the optimisation of the chemical structure (Supplementary Information 1). **B** The stability of coatings was studied using FTIR. FEP FTIR spectrum (top red) was compared to those of the coatings immediately, after 1 week, 2 weeks, one month and two months (from green top to bottom

predict pH values from both the xy-position in the image and the collection of fluorescent responses from all four excitation wavelengths (Fig. 4B & C). Results showed the machine learning approach improved predictions significantly in a test dataset (Fig. 4C, $t=79.9$, $p<0.001$), with 95% of the predictions falling within -0.4 and 0.3 units of the true pH value, almost doubling the precision of the ratiometric fluorescence predictions. Ratiometric fluorescence predictions also introduced bias leading to underestimation of large pH values (supplementary Fig. S2). Up to 80% of variation in pH was correctly predicted using neural networks with only 46% of the variance explained by the ratiometric fluorescence approach.

black respectively). **C** The particles were tested for imaging using light sheet scattering (blue) and fluorescence (green) signals (scale bar 1 mm). **D** Water contact angle measurement of FEP (hydrophobic, > 90 , left), and that of the functional polymer (hydrophilic, < 90 , right). **E** Water retention of the terpolymers containing PEGMA (red x) increased the water retention of FEP soil particles (cyan +) with comparison to virgin FEP particles (blue Δ). van Genuchten curves (dashed lines) for gravel (Tokunaga et al. 2002), sand, sandy loam and loam soils (Šimůnek et al. 2006) are given for comparison. Shaded areas indicate mean value \pm SE for smart soil and the range of values observed in natural sandy soils

Smart soil particles help understand the formation of soil chemical heterogeneity

Using the fabricated smart soil particles, pH dynamics in the rhizosphere of plants were observed up to one week after germination. The first indication of root driven pH change was visible after 4 days (data not shown). Following growth in the smart soils, we could observe changes in chemical properties by the naked eye (Fig. 5A) and subsequently analyse how these changes relate to soil and root biological activity. Maps of entire seedlings and surrounding smart soils were assembled by tessellating images to produce volume data corresponding to up to 3 cm^3 of substrate at $10 \mu\text{m}$ resolution with each time point

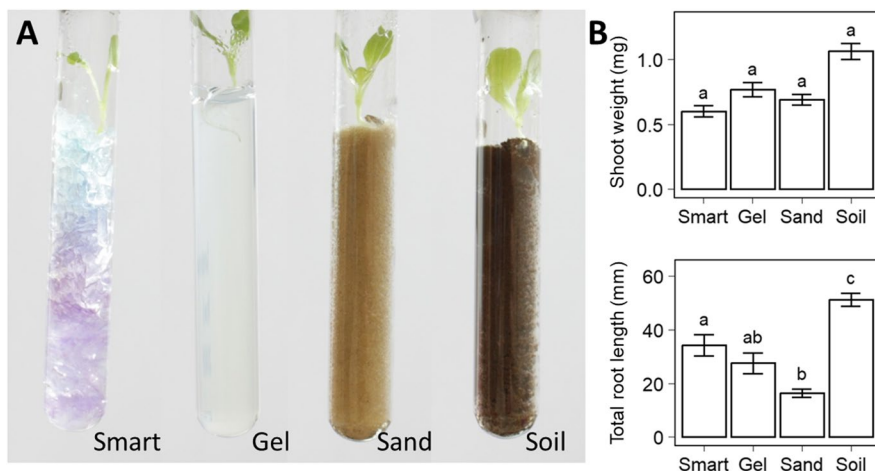
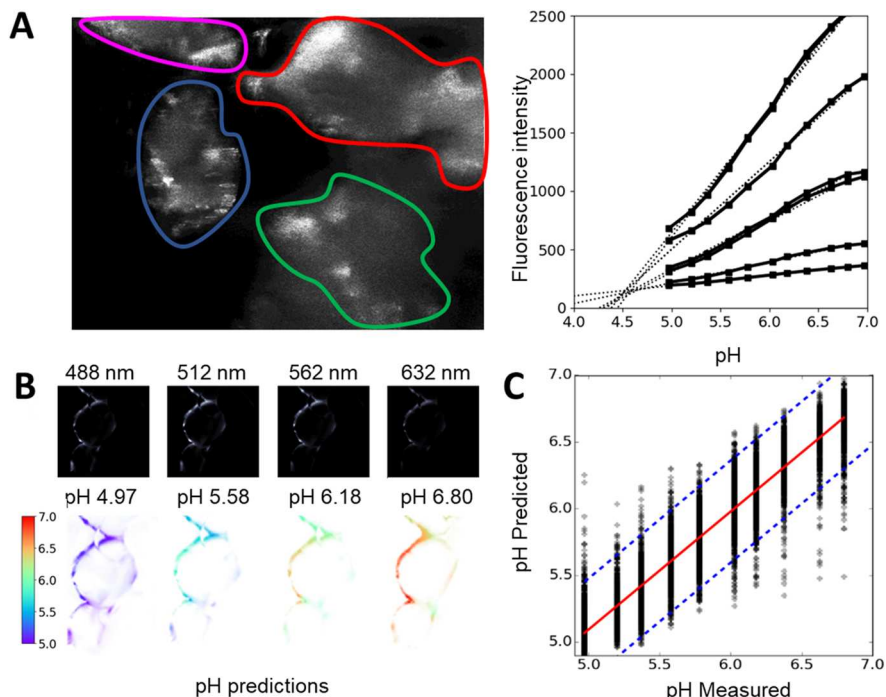


Fig. 3 Biocompatibility of smart soil particles. **A** Growth of lettuce seedling in chunk FEP particles (Smart), water agar (Gel), fine sand (Sand) and an agricultural soil (Soil). **B** Effect of the nature of substrate on shoot biomass (top) and root biomass (bottom). An analysis of variance showed root length but

not shoot weight were significantly affected by soil treatments ($p < 0.05$). Error bars indicate mean value \pm SE for artificial soil and the range of values observed in natural sandy soils; Tukey codes from post-hoc tests are given where different letters denote statistically different means

Fig. 4 Calibration of pH sensing particles. **A** Change of the green fluorescence (488 nm / 530 nm) from individual particles (here shown in outlines of different colours) in response to a change in pH from 5 to 7 showing linear responses to pH but strong variations in the slope of the response. **B** The machine learning approach utilised data from four fluorescence signals to predict pH in situ from light sheet microscopy. Pseudo colours indicate pH predictions corresponding to the pH buffer used (indicated above each image). **C** pH predictions using the machine learning approach explained up to 80% of the variance of the data and exhibited limited bias



producing a dataset of approximately 4 Gb. pH predictions obtained from the data acquired 7 days after inoculation (Fig. 5B-D) revealed how soil chemical heterogeneity may form as a result of root exudation,

and how this process is influenced by the generation of microsites and the type of FEP particles. Non-linear mixed effect models (Supplementary Information 2) showed that when roots grew in smart soil

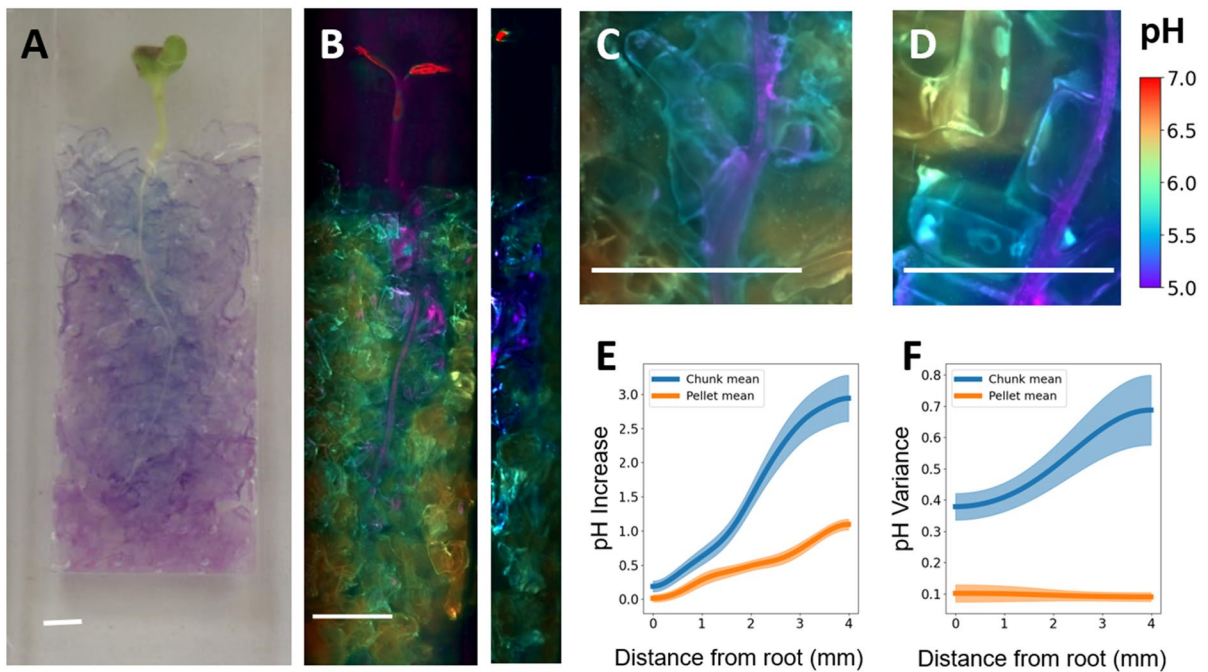


Fig. 5 Smart particles reveal how interaction between root exudation and particle type affects the chemical heterogeneity of soils. **A** Seedlings grown in chunk FEP particles induced changes in colours of particles due to acidification. **B** Estimation of pH values from light sheet microscopy data revealed the pH distribution in the inner soil (max projection on the left, cross section on the right, scale bar of 4 mm). High resolution view of example images of roots from which data was acquired on two types of soils, chunk FEP particles (**C**) and pellet FEP

particles (**D**) represented with a scale bar of 4 mm. **E** Change in pH as a function of the distance from the root surface for chunk FEP particles (blue) and pellet FEP particles (orange). **F** pH variance as a function of the distance from the root surface for chunk FEP particles (blue) and pellet FEP particles (orange). Non-linear mixed effect models showed the pH response observed in the two soils was statistically different ($\chi^2=1612.45$, $p<0.001$). Confidence intervals indicate mean value \pm SE.

made of chunk FEP particles (factory waste), the pH increased by 2.65 over a distance of approximately 2 mm from the root (scale parameter 0.51 in sigmoid growth). In contrast, the increase of pH around roots grown in smart soil made of pellet FEP particles (virgin material prior to melt processing) was limited to 0.87 and this was observed at greater distance than in smart soil made of chunk FEP particles (scale factor 0.65, Fig. 5E). Application of the Likelihood Ratio tests ($\chi^2=1612.45$, $p<0.001$) showed this trend was highly significant. Chunk FEP particles also produced a more heterogeneous chemical environment with variance increasing with distance from the root (Fig. 5F) and therefore equated more closely to the properties of natural soils.

Discussion

The challenges of the fabrication of smart soils

This work successfully recorded the 3D pH gradients that form within the pores of the space surrounding growing plant roots. A crucial step in achieving this result was the functionalization of FEP particles. Enhancing the properties of such specialised fluoropolymers is challenging because of their lack of reactivity, but we have developed a three step-strategy to overcome these difficulties. The synthesis of functional polymers is first optimised without the core for characterisation of chemical, physical and optical properties. Synthesis is followed by fast

particle prototyping using Fluorine-Fluorine interaction (Baker et al. 2012; Pigiaccielli et al. 2022) to coat FEP particles and allowing the blending of polymers or the recovery of the polymers tested for reuse. Production of the final prototype could then be achieved by radiografting polymerisation (Dargaville et al. 2003) for long term stability of the particle. Here such a graft polymerisation of the functional polymer was successfully tested on FEP particles, but not presented because it did not produce enough substrate for the study. Finally, reusability, cost and the possibility to use waste material, which is not recycled in the case of FEP (Dams and Hintzer 2016), will be important technological considerations for future development of smart soils. This study has also established the possibility of using factory waste for the fabrication of smart soils.

The development of this first generation of smart soils also gave indications on the limitations of current fabrication techniques. Results showed that surface attachment and coating stability require the introduction of an additional monomer(s), making the synthesis more complex and costly. The future development of graft polymerisation (Ruckenstein and Li 2005) could both significantly improve the number of uses of smart soils and reduce the quantity of functional polymers needed for fabrication. Combining sufficient ion exchange and water retention capacity within each individual particle was challenging because the ionic strength of acid groups could not offset the strong hydrophobic nature of fluoropolymers. The water contact angle of the surface of the particles were reduced from 112° to as low as 88° using 2-trifluoromethacrylic acid (MAF), and these results are similar to other available techniques such as H₂ or O₂ plasma etching (Park et al. 2002) and water retention of coarse sand was achieved. Oligo(ethylene glycol) made surfaces highly hydrophilic (46°) but did not provide any surface charge for binding of mineral ions.

This work did not study the processing of FEP into particles. FEP particles were generated at the supplier's premises by shredding FEP films. Even when complemented by sieving, the resulting granular medium did not produce particles whose longest axis was below 2 mm. In addition, the particles typically have flake-like shapes which did not mimic well the granular properties of natural soils. Finally, fabrication techniques proposed in this study are suitable to

produce only a few grams of smart soil in one run. The coating of the particles was the main bottleneck in the fabrication pipeline and was limited by the size of the flask of the rotary evaporator. However, scaling this process up is achievable using industrial coating techniques such as spray coating (Turton and Cheng 2005).

Using smart soil to study rhizosphere dynamics

The utilization of our new technology has revealed characteristics of pH changes induced by root exudation at a far higher resolution than was previously possible with techniques such as planar optodes or zymography assays (Blossfeld and Gansert 2007; Giles et al. 2018) This advancement enables the possibility of reconstructing the spatial structure of chemical gradients in samples of small size. Prior to this study, current non-destructive imaging techniques had not provided real-time observations of chemical or biological activity in situ within soil.

We also quantitatively analyzed the pH change occurring along the root. We measured pH variations within a diameter of approximately 1 cm around the roots and observed that acidification occurred within 2–3 mm from the root surface, which is consistent with previous observations in natural soils (Jones et al. 2004; Koop-Jakobsen et al. 2018; Sun et al. 2019). We could also produce smart soil with different structure and observed that chemical changes induced by the roots are intimately related to the structure of the granular media itself. Smaller particles introduced more variable conditions around the root, perhaps due to reduced diffusion coefficients and more tortuous diffusion pathways interacting with variation in exudation patterns.

Our results also revealed current limitations of using artificial substrates as substitutes for natural soils. Although surfaces of smart soil particles were highly hydrophilic (Fig. 2), the particle size distributions of smart soils were too coarse to match the water retention from a sand. The irregular shapes of the chunk FEP smart particles occasionally formed large pores which resulted in a porosity of about 75%, which is larger than most soils (Morris and Johnson 1967). The chemistry of the surface of soil particles is equally difficult to optimise. The surface of natural soil particles is chemically diverse and adsorbs ions in complex ways. Typical examples include the

fixation of phosphate which can be achieved by different oxides, hydroxides and clay surfaces (Barrow 2017), or the adsorption of potassium which can be either in exchangeable form or fixed between mineral layers (Zhang et al. 2009). Achieving such binding specificity is challenging, and only ion exchange capacity has been demonstrated so far (Downie et al. 2012).

The ability of the smart soil to generate optical signals through live microscopy is also critical for the observation of rhizosphere processes. In this study, we noted that the quality of the signals was primarily affected by the particle size distribution and water content. The best signal was acquired during calibration when particles were isolated and completely saturated in the buffer solution (Fig. 4B). However, the air left in the pores degraded the signal significantly. The degradation is due to reflection and diffraction at air-liquid interfaces, which affects both excited and emitted light. When using smart soils made of pellets, there were fewer air-liquid interfaces and thus the variability of the calculated pH values was limited. However, when using smart soils made of chunk FEP particles, we observed a decline in accuracy and significant variability in the calculated pH, in some cases leading to atypical pH values (Fig. 5). The scattering of the FEP particle could be detected by the microscope (Fig. 2) but its effect was less important than that caused by air. To limit the artefacts in this initial study, we chose to perform the study with both sterilised smart soil and seed and also to work with thin layers of soil (3 mm thickness). Improving light transmittance by saturating the volume with water enabled imaging through samples that are centimetres in size (Martins et al. 2019), but this can significantly affect diffusion and pH distribution in the substrate. Developing more transparent FEP alternatives seems unrealistic in the short term because of the difficulty in synthesizing polymers with high fluorine content.

New materials and technologies for the next generation of smart soils

New materials and technologies offer huge opportunities to further enhance the capabilities of smart soil particles, for example improving the wettability of the particles using polymer brush structures (Zahner et al. 2011; Kobayashi et al. 2012), optimising the

porosity of polymers (Vos et al. 2013) or the roughness of surfaces (Tokunaga 2009). Materials could also be engineered to mimic more closely the binding of mineral elements and pH dependence of surface properties. Microfabrication techniques could be used to engineer the size and shapes of particles with a high precision (Aufrecht et al. 2022) and to better control environmental conditions in microcosm experiments (Stanley et al. 2018). More realistic biotic environments could also be obtained by combining synthetic communities of bacteria (Herrera Paredes et al. 2018) and soil organic matter. The scaling up of fabrication processes will result in large volume of substrates available for experiments and growing of larger plants for longer periods of time. Attaching sensors to monitor oxygen (Bitig et al. 2018) and nutrient concentration (Strömberg 2008) would in turn improve the understanding of the formation and diversity of rhizosphere microhabitats. Finally, improved image processing algorithms could considerably enhance the accuracy of measurements, bypassing noise and artifact and extracting the relevant parts of the soil volume for prediction and analysis (Schlüter et al. 2022). Smart soil technologies are bringing unique new capabilities to monitor and quantify biological and chemical processes in the rhizosphere, and in the future, they could help drive understanding of soil biogeochemical processes and promote new forms of agronomic screening in industry.

Acknowledgements This work was funded by the European Research Council (ERC) under the European Union's Horizon 2020 research and innovation programme (Grant agreement No. 647857-SENSOILS). We also acknowledge the funding from the Spanish Ministry of Science and Innovation (MICINN) under de project MICROCROWD (PID2020-112950RR-I00). Researchers at the James Hutton Institute also receive financial support from the Rural & Environment Science & Analytical Services Division of the Scottish Government. The authors thank Akzo and Tosoh Finechemicals Corp. for supplying with *tert*-butyl peroxyphthalate and 2-trifluoromethacrylic acid, respectively. BA also thanks the French Fluorine Network (GIS).

Author contributions Conceptualization: LXD, BA, VL, MPM, TJD

Methodology: LXD, BA, VL, MPM, TSG

Investigation: DP, QY, PF, YH, BB, BVT

Funding: acquisition: LXD

Project administration: LXD

Supervision: LXD, BA, TSG, TJD, VL, MPM

Writing – original draft: DP, QY, PF, YH, LXD

Writing – review & editing: BA, VL, MPM, TSG, TJD

Data availability Software developed for predicting pH from image data is available at https://github.com/LionelDupuy/SENSOIL/tree/main/pH_Release.

Declarations

Competing interest There is no competing interest.

Open Access This article is licensed under a Creative Commons Attribution 4.0 International License, which permits use, sharing, adaptation, distribution and reproduction in any medium or format, as long as you give appropriate credit to the original author(s) and the source, provide a link to the Creative Commons licence, and indicate if changes were made. The images or other third party material in this article are included in the article's Creative Commons licence, unless indicated otherwise in a credit line to the material. If material is not included in the article's Creative Commons licence and your intended use is not permitted by statutory regulation or exceeds the permitted use, you will need to obtain permission directly from the copyright holder. To view a copy of this licence, visit <http://creativecommons.org/licenses/by/4.0/>.

References

- Alcantar NA, Aydil ES, Israelachvili JN (2000) Polyethylene glycol-coated biocompatible surfaces. *J Biomed Mater Res An Off J Soc Biomater Japanese Soc Biomater Aust Soc Biomater Korean Soc Biomater* 51:343–351
- Ameduri B, Fomin S (2020) Fascinating fluoropolymers and their applications. Elsevier, Oxford, UK
- Aufrecht J, Khalid M, Walton CL et al (2022) Hotspots of root-exuded amino acids are created within a rhizosphere-on-a-chip. *Lab Chip* 22:954–963
- Baker RJ, Colavita PE, Murphy DM et al (2012) Fluorine-fluorine interactions in the solid state: an experimental and theoretical study. *J Phys Chem A* 116:1435–1444. <https://doi.org/10.1021/jp2099976>
- Baldini F, Chester AN, Homola J, Martellucci S (2006) Optical chemical sensors. Springer, Dordrecht
- Barrow NJ (2017) The effects of pH on phosphate uptake from the soil. *Plant Soil* 410:401–410. <https://doi.org/10.1007/s11104-016-3008-9>
- Bittig HC, Körtzinger A, Neill C et al (2018) Oxygen optode sensors: principle, characterization, calibration, and application in the ocean. *Front Mar Sci* 4:1–25. <https://doi.org/10.3389/fmars.2017.00429>
- Blossfeld S, Gansert D (2007) A novel non-invasive optical method for quantitative visualization of pH dynamics in the rhizosphere of plants. *Plant Cell Environ* 30:176–186. <https://doi.org/10.1111/j.1365-3040.2006.01616.x>
- Burr-Hersey JE, Ritz K, Bengough GA, Mooney SJ (2020) Reorganisation of rhizosphere soil pore structure by wild plant species in compacted soils. *J Exp Bot* 71:6107–6115
- Clark LJ, Whalley WR, Leigh RA, Dexter AR, Barraclough PB (1999) Evaluation of agar and agarose gels for studying mechanical impedance in rice roots. *Plant Soil* 207:37–43
- Dams R, Hintzer K (2016) Industrial aspects of fluorinated oligomers and polymers. In: Ameduri B, Sawada H (eds) *Fluorinated polymers*, vol 2. applications. Royal Society of Chemistry, Chambridge, pp 1–31
- Dargaville TR, George GA, Hill DJT, Whittaker AK (2003) High energy radiation grafting of fluoropolymers. *Prog Polym Sci* 28:1355–1376
- Downie H, Holden N, Otten W et al (2012) Transparent soil for imaging the rhizosphere. *PLoS ONE* 7:1–6. <https://doi.org/10.1371/journal.pone.0044276>
- Duncan KE, Czymmek KJ, Jiang N et al (2022) X-ray microscopy enables multiscale high-resolution 3D imaging of plant cells, tissues, and organs. *Plant Physiol* 188:831–845. <https://doi.org/10.1093/plphys/kiab405>
- DuPont (2013) Fluoroplastic film properties bulletin. DuPont, Wilmington
- Ebnesajjad S (2015) Fluoroplastics, volume 2: melt processible fluoroplastics. William Andrew, Amsterdam
- Engelhardt IC, Patko D, Liu Y et al (2022) Novel form of collective movement by soil bacteria. *ISME J* 16:2337–2347. <https://doi.org/10.1038/s41396-022-01277-w>
- Ge S, Dong X, Liu Y et al (2023) In situ control of root–bacteria interactions using optical trapping in transparent soil. *J Exp Bot* 74:787–799. <https://doi.org/10.1093/jxb/erac437>
- Ge S, Dupuy LX, MacDonald MP (2021) In situ laser manipulation of root tissues in transparent soil. *Plant Soil* 468:475–489. <https://doi.org/10.1007/s11104-021-05133-2>
- Giles CD, Dupuy L, Boitt G et al (2018) Root development impacts on the distribution of phosphatase activity: improvements in quantification using soil zymography. *Soil Biol Biochem* 116:158–166. <https://doi.org/10.1016/j.soilbio.2017.08.011>
- Han C, Ren J, Tang H et al (2016) Quantitative imaging of radial oxygen loss from *Valisneria spiralis* roots with a fluorescent planar optode. *Sci Total Environ* 569:1232–1240
- Henry BJ, Carlin JP, Hammerschmidt JA et al (2018) A critical review of the application of polymer of low concern and regulatory criteria to fluoropolymers. *Integr Environ Assess Manag* 14:316–334
- Herrera Paredes S, Gao T, Law TF et al (2018) Design of synthetic bacterial communities for predictable plant phenotypes. *PLoS Biol* 16:e2003962
- Hoell D, Mensing T, Roggenbuck R et al (2012) 2-Butanone. Ullmann's Encyclopedia of Industrial Chemistry, 7th edn. Wiley, New York
- Hougham G, Cassidy PE, Johns K, Davidson J (1999) Fluoropolymers: synthesis and applications. Plenum Press, New York
- Huber C, Klimant I, Krause C et al (2001) Nitrate-selective optical sensor applying a lipophilic fluorescent potential-sensitive dye. *Anal Chim Acta* 449:81–93. [https://doi.org/10.1016/S0003-2670\(01\)01363-0](https://doi.org/10.1016/S0003-2670(01)01363-0)
- Jol HM (2008) Ground penetrating radar theory and applications. Elsevier Science, Amsterdam
- Jones DL, Hodge A, Kuzyakov Y (2004) Plant and mycorrhizal regulation of rhizodeposition. *New Phytol* 163:459–480
- Kobayashi M, Terayama Y, Yamaguchi H et al (2012) Wettability and antifouling behavior on the surfaces of superhydrophilic polymer brushes. *Langmuir* 28:7212–7222
- Koebnick N, Daly KR, Keyes SD et al (2019) Imaging microstructure of the barley rhizosphere: particle packing and

- root hair influences. *New Phytol* 221:1878–1889. <https://doi.org/10.1111/nph.15516>
- Koop-Jakobsen K, Mueller P, Meier RJ et al (2018) Plant-sediment interactions in salt marshes: an optode imaging study of O₂, pH, and CO₂ gradients in the rhizosphere. *Front Plant Sci* 9:541
- Kopittke PM, Menzies NW (2004) Effect of Mn deficiency and legume inoculation on rhizosphere pH in highly alkaline soils. *Plant Soil* 262:13–21
- Korenblum E, Dong Y, Szymanski J et al (2020) Rhizosphere microbiome mediates systemic root metabolite exudation by root-to-root signaling. *Proc Natl Acad Sci U S A* 117:3874–3883. <https://doi.org/10.1073/pnas.1912130117>
- Liu Y, Patko D, Engelhardt I et al (2021) Plant–environment microscopy tracks interactions of *Bacillus subtilis* with plant roots across the entire rhizosphere. *Proc Natl Acad Sci* 118:e2109176118. <https://doi.org/10.1073/pnas.2109176118>
- Lookadoo DB, Schönhorn JE, Harpaldas H et al (2021) Based Optode Devices (PODs) for selective quantification of potassium in biological fluids. *Anal Chem* 93:9383–9389
- Ma L, Shi Y, Siemianowski O et al (2019) Hydrogel-based transparent soils for root phenotyping in vivo. *Proc Natl Acad Sci U S A* 166:11063–11068. <https://doi.org/10.1073/pnas.1820334116>
- Martins AD, O’Callaghan F, Bengough AG, Loades KW, Pasqual M, Kolb E, Dupuy LX (2020) The helical motions of roots are linked to avoidance of particle forces in soil. *New Phytol* 225:2356–2367
- Moradi AB, Carminati A, Vetterlein D et al (2011) Three-dimensional visualization and quantification of water content in the rhizosphere. *New Phytol* 192:653–663. <https://doi.org/10.1111/j.1469-8137.2011.03826.x>
- Morris DA, Johnson AI (1967) Summary of hydrologic and physical properties of rock and soil materials, as analyzed by the hydrologic laboratory of the U.S. Geological Survey, 1948–60. U.S. Government Printing Office. <https://doi.org/10.3133/wsp1839D>
- O’Callaghan FE, Braga RA, Neilson R et al (2018) New live screening of plant-nematode interactions in the rhizosphere. *Sci Rep* 8:1840. <https://doi.org/10.1038/s41598-017-18797-7>
- Oburger E, Jones DL (2018) Sampling root exudates—mission impossible? *Rhizosphere* 6:116–133
- Okamoto Y, Mikeš F, Koike K, Koike Y (2014) Amorphous Perfluoropolymers. *Handbook of Fluoropolymer Science and Technology*. Wiley Blackwell, New York, pp 377–391. <https://doi.org/10.1002/9781118850220.ch16>
- Panini P, Chopra D (2015) Understanding of noncovalent interactions involving organic fluorine. In: Li Z, Wu L (eds) *Hydrogen Bonded Supramolecular Structures*. Springer Verlag, Berlin, pp 37–67
- Park YW, Tasaka S, Inagaki N (2002) Surface modification of tetrafluoroethylene–hexafluoropropylene (FEP) copolymer by remote H₂, N₂, O₂, and Ar plasmas. *J Appl Polym Sci* 83:1258–1267
- Pedregosa F, Varoquaux G, Gramfort A et al (2011) Scikit-learn: machine learning in Python. *J Mach Learn Res* 12:2825–2830
- Pigliacelli C, Acocella A, Díez I et al (2022) High-resolution crystal structure of a 20 kDa superfluorinated gold nanocluster. *Nat Commun* 13. <https://doi.org/10.1038/s41467-022-29966-2>
- Pinheiro J, Bates D, DebRoy S et al (2013) nlme: linear and nonlinear mixed effects models. R Packag version 3:111
- Plett KL, Buckley S, Plett JM et al (2021) Novel microdialysis technique reveals a dramatic shift in metabolite secretion during the early stages of the interaction between the ectomycorrhizal fungus *Pisolithus microcarpus* and its host *Eucalyptus grandis*. *Microorganisms* 9:1817
- Ruckenstein E, Li ZF (2005) Surface modification and functionalization through the self-assembled monolayer and graft polymerization. *Adv Colloid Interface Sci* 113:43–63
- Rudolph-Mohr N, Bereswill S, Tötze C et al (2021) Neutron computed laminography yields 3D root system architecture and complements investigations of spatiotemporal rhizosphere patterns. *Plant Soil* 469:489–501
- Schlüter S, Leuther F, Albrecht L et al. (2022) Microscale carbon distribution around pores and particulate organic matter varies with soil moisture regime. *Nat Commun* 13. <https://doi.org/10.1038/s41467-022-29605-w>
- Sharma K, Palatinszky M, Nikolov G et al (2020) Transparent soil microcosms for live-cell imaging and non-destructive stable isotope probing of soil microorganisms. *Elife* 9:e56275
- Šimůnek J, van Genuchten MT, Šejna M (2006) The HYDRUS software package for simulating the two- and three-dimensional movement of water, heat, and multiple solutes in variably-saturated media. Technical manual, version, 1, 241
- Stanley CE, Shrivastava J, Brugman R et al (2018) Fabrication and use of the dual-flow-rootchip for the imaging of Arabidopsis roots in asymmetric microenvironments. *Bio-protocol* 8:e3010–e3010
- Strömberg N (2008) Determination of ammonium turnover and flow patterns close to roots using imaging optodes. *Environ Sci Technol* 42:1630–1637. <https://doi.org/10.1021/es071400q>
- Sun X, Li Z, Wu L et al (2019) Root-induced soil acidification and cadmium mobilization in the rhizosphere of *Sedum plumbizincicola*: evidence from a high-resolution imaging study. *Plant Soil* 436:267–282
- Tokunaga TK (2009) Hydraulic properties of adsorbed water films in unsaturated porous media. *Water Resour Res* 45:1–9. <https://doi.org/10.1029/2009WR007734>
- Tokunaga TK, Wan J, Olson KR (2002) Saturation-matric potential relations in gravel. *Water Resour Res* 38:32. <https://doi.org/10.1029/2001wr001242>
- Turton R, Cheng XX (2005) The scale-up of spray coating processes for granular solids and tablets. *Powder Technol* 150:78–85
- Van der Meeren P, De Vleeschouwer D, Debergh P (2001) Determination of oxygen profiles in agar-based gelled in vitro plant tissue culture media. *Plant Cell Tissue Organ Cult* 65:239–245. <https://doi.org/10.1023/A:1010698225362>

- Van Veelen A, Koebernick N, Scotson CS et al (2020) Root-induced soil deformation influences Fe, S and P: rhizosphere chemistry investigated using synchrotron XRF and XANES. *New Phytol* 225:1476–1490
- Vos M, Wolf AB, Jennings SJ, Kowalchuk GA (2013) Micro-scale determinants of bacterial diversity in soil. *FEMS Microbiol Rev* 37:936–954
- Zahner D, Abagat J, Svec F et al (2011) A facile approach to superhydrophilic–superhydrophobic patterns in porous polymer films. *Adv Mater* 23:3030–3034
- Zappala S, Helliwell JR, Tracy SR et al (2013) Effects of X-ray dose on rhizosphere studies using X-ray computed tomography. *PLoS ONE* 8:e67250
- Zhang H, Xu M, Zhang W, He X (2009) Factors affecting potassium fixation in seven soils under 15-year long-term fertilization. *Chin Sci Bull* 54:1773–1780. <https://doi.org/10.1007/s11434-009-0164-9>

Publisher's note Springer Nature remains neutral with regard to jurisdictional claims in published maps and institutional affiliations.